Incomplete erasure of histone marks during epigenetic reprogramming in medaka early development

Hiroto S. Fukushima, Hiroyuki Takeda and Ryohei Nakamura

Genome Res. 2023 33: 572-586 originally published online April 28, 2023
Access the most recent version at doi:10.1101/gr.277577.122

Incomplete erasure of histone marks during epigenetic reprogramming in medaka early development

Hiroto S. Fukushima, Hiroyuki Takeda, and Ryohei Nakamura

Department of Biological Sciences, Graduate School of Science, The University of Tokyo, Tokyo 113-0033, Japan

Epigenetic modifications undergo drastic erasure and reestablishment after fertilization. This reprogramming is required for proper embryonic development and cell differentiation. In mammals, some histone modifications are not completely reprogrammed and play critical roles in later development. In contrast, in nonmammalian vertebrates, most histone modifications are thought to be more intensively erased and reestablished by the stage of zygotic genome activation (ZGA). However, histone modifications that escape reprogramming in nonmammalian vertebrates and their potential functional roles remain unknown. Here, we quantitatively and comprehensively analyzed histone modification dynamics during epigenetic reprogramming in Japanese killifish, medaka (*Oryzias latipes*) embryos. Our data revealed that H3K27ac, H3K27me3, and H3K9me3 escape complete reprogramming, whereas H3K4 methylation is completely erased during cleavage stage. Furthermore, we experimentally showed the functional roles of such retained modifications at early stages: (i) H3K27ac premarks promoters during the cleavage stage, and inhibition of histone acetyltransferases disrupts proper patterning of H3K4 and H3K27 methylation at CpG-dense promoters, but does not affect chromatin accessibility after ZGA; (ii) H3K9me3 is globally erased but specifically retained at telomeric regions, which is required for maintenance of genomic stability during the cleavage stage. These results expand the understanding of diversity and conservation of reprogramming in vertebrates, and unveil previously uncharacterized functions of histone modifications retained during epigenetic reprogramming.

[Supplemental material is available for this article.]

After fertilization, the epigenetic landscapes of sperm and oocyte chromosomes undergo drastic erasure and reestablishment to ensure totipotency and/or pluripotency in early embryos (Eckersley-Maslin et al. 2018; Xia and Xie 2020). In mice, DNA methylation and histone modifications transmitted from parental germ cells are globally reset in early embryos. However, some modifications are known to persist and play essential roles in later development (Xia and Xie 2020). Such examples include DNA methylation at specific gene loci passed on to imprinted genes (Eckersley-Maslin et al. 2018) and the asymmetric pattern of the heterochromatin mark H3K9me3 retained until the blastocyst stage (Wang et al. 2018). Furthermore, a noncanonical pattern of the active mark H3K4me3 established in oocytes is transferred to the zygote and exists until zygotic genome activation (ZGA) (Dahl et al. 2016; Zhang et al. 2016). Additionally, the repressive mark H3K27me3 transmitted from oocytes regulates DNA methylation-independent imprinting in embryos (Inoue et al. 2017).

Epigenetic reprogramming of nonmammalian vertebrates is largely distinct from that of mammals. DNA methylation does not undergo genome-wide demethylation, and is largely maintained (Macleod et al. 1999; Veenstra and Wolffe 2001; Jiang et al. 2013; Potok et al. 2013). In contrast, histone modifications are more extensively erased in early embryos of nonmammalian vertebrates (Xia and Xie 2020). Importantly, unlike in mammals, ZGA and subsequent cell differentiation occur after a number of cell divisions (e.g., around ten cell cycles in zebrafish and *Xenopus*) in nonmammalian vertebrate embryos (Jukam et al. 2017), and the reprogramming of histone modifications takes place well before ZGA. For example, in zebrafish and *Xenopus*, H3K4me3, H3K27me3, and H3K9me3 were reported to be almost completely absent before ZGA, but these marks start accumulating at the onset or shortly before the ZGA (Akkers et al. 2009; Vastenhouw et al. 2010; Lindeman et al. 2011; Hontelez et al. 2015; Zhang et al. 2018a; Laue et al. 2019). Thus, parental histone modifications are less likely to be transmitted nor maintained through cleavage stages, and to affect later development in nonmammalian vertebrates. However, this notion has been challenged by recent studies.

In zebrafish, nucleosomes with H3K4me1 and H2A.Z (so-called "Placeholder nucleosomes") were suggested to persist after fertilization to premark active and poised promoters (Murphy et al. 2018; Hickey et al. 2022). Additionally, Zhang et al. revealed that H3K27ac accumulates in four-cell-stage zebrafish embryos and could play a role in priming gene promoters for later ZGA (Zhang et al. 2018a), raising the possibility that some histone modifications are maintained before ZGA and required for later development in nonmammalian vertebrates. However, these studies relied on immunofluorescence staining or conventional chromatin immunoprecipitation sequencing (ChIP-seq) to show the presence of histone modifications in early embryos, both of which do not allow quantitative comparison of histone modifications at each genomic locus at different developmental stages (Bonhoure et al. 2014; Li et al. 2014; Orlando et al. 2014). Thus, it remains to be elucidated exactly to what extent each histone modification is retained during the epigenetic reprogramming of

Corresponding authors: htakeda@bs.s.u-tokyo.ac.jp, rynakamura@bs.s.u-tokyo.ac.jp
Article published online before print. Article, supplemental material, and publication date are at https://www.genome.org/cgi/doi/10.1101/gr.277577.122.

33:572–586 Published by Cold Spring Harbor Laboratory Press; ISSN 1088-9051/23; www.genome.org

nonmammalian vertebrates, and if some modifications are retained, whether they affect the phenotype of offspring. Moreover, recent studies revealed that epigenetic patterns are very diverse even in mammals (Xia et al. 2019; Lu et al. 2021). Due to the limited number of studies performed so far, it is not fully understood to what degree the reprogramming process of histone modifications is conserved or diverse among vertebrates.

To obtain quantitative, comprehensive, and evolutionarily comparative data, we chose medaka, Japanese killifish (*Oryzias latipes*), which has a number of advantages in the study of genome and epigenome such as small genome size (800 Mb) (Takeda and Shimada 2010), high-quality reference genome sequence (Ichikawa et al. 2017), accumulated epigenome data (Nakamura et al. 2014, 2021; Li et al. 2020), and instances of transgenerational epigenetic inheritance (Bhandari 2016) with a large evolutional distance to other vertebrate models (e.g., medaka vs. zebrafish: ~115–200 million years; fish vs. *Xenopus*: ~450 million years; *Xenopus* vs. mammals: ~350 million years; mouse vs. human: ~80 million years) (Furutani-Seiki and Wittbrodt 2004). We quantitatively validated the epigenetic reprogramming of histone modifications in medaka early embryos by conducting quantitative ChIP-seq (Bonhoure et al. 2014; Li et al. 2014; Orlando et al. 2014), together with immunofluorescence staining. We also experimentally examined function of modifications retained during epigenetic reprogramming.

Results

Erasure and retention of histone modifications before ZGA in medaka embryos shown by immunofluorescence staining

Like other nonmammalian vertebrates (Jukam et al. 2017), medaka embryos undergo rapid and synchronous cell cycles after fertilization, and cell division gradually becomes longer and asynchronous from the late morula stage (stage 9, 256–512 cells) (Fig. 1A; Supplemental Fig. S1). ZGA occurs from the early blastula stage (stage 10, ~1000 cells) (Nakamura et al. 2021). Blastomeres are pluripotent until the late blastula stage (stage 11, 2000–4000 cells) (Kinoshita et al. 2009), but thereafter cell differentiation begins and three germ layers emerge from the pre-early gastrula stage onwards (stage 12) (Fig. 1A).

As a first step toward understanding of when and how histone modifications are reprogrammed in medaka early development, we performed immunofluorescence staining of embryos using antibodies against various histone modifications (H3K27ac, H3K27me3, H3K9me3, H3K4me1, H3K4me2, and H3K4me3) at the 16-cell, 64-cell, late morula, and late blastula stages (Fig. 1B, C). First, we found that among the active marks, H3K27ac was detected at all four stages examined, but other active marks (H3K4me1, H3K4me2, and H3K4me3) were not detected until the late morula stage (Fig. 1B,C). H3K4 methylation became weakly detectable at the late morula stage and clearly accumulated at the late blastula stage (Fig. 1B,C). The absence of H3K4 methylation after fertilization is consistent with previous studies in zebrafish (Vastenhouw et al. 2010; Lindeman et al. 2011).

Second, the repressive H3K27me3 and H3K9me3 marks were only detected in mitotic phase chromatin at the 16-cell, 64-cell, and late morula stages, but detected in both mitotic phase and interphase chromatin at the late blastula stage (Fig. 1B,C). This suggests that H3K27me3 and H3K9me3 mostly accumulate during or after ZGA, consistent with previous studies in zebrafish and *Xenopus* (Akkers et al. 2009; Zhang et al. 2018a; Laue et al. 2019), but the two modifications exist at low levels before ZGA, so that they can be detected in compact mitotic chromosome in medaka. We speculated that chromatin compaction during the mitotic phase increased the signal intensity, compared to the dispersed signal observed in interphase nuclei, because the H3K27ac signal in mitotic phases also tended to be higher than that in interphase (Fig. 1B,C).

Importantly, the immunofluorescence signals of H3K27ac, H3K27me3, and H3K9me3 were almost completely eliminated by treatment with A485, a specific inhibitor of H3K27ac histone acetyltransferases Crebbp and Ep300 (also known as Cbp and P300, encoded by *crebbpa*, *crebbpb*, *ep300a*, and *ep300b* genes in medaka, hereafter we simply referred to them as Crebbp/Ep300) (Supplemental Fig. S16A,B; Lasko et al. 2017; Hogg et al. 2021; Narita et al. 2021; Pelham-Webb et al. 2021), overexpression of a medaka H3K27me3 demethylase *kdm6ba* (*Oryzias latipes* Kdm6ba, olKdm6ba) (Supplemental Fig. S2A–C; Agger et al. 2007; Inoue et al. 2017; Jullien et al. 2017), and overexpression of a human H3K9me3 demethylase *KDM4D* (*Homo sapiens* KDM4D, hsKDM4D) (Fig. 4A,B; Supplemental Fig. S11A; Matoba et al. 2014; Jullien et al. 2017; Zhang et al. 2018b), respectively. Essentially, no positive signal was observed in immunofluorescence staining using IgG as a negative control (Supplemental Figs. S2D, S10B). These results supported the conclusion that the immunofluorescence staining signals of histone modifications during epigenetic reprogramming were specific. Furthermore, one-cell-stage embryos showed positive signals for all histone modifications examined in this study (Supplemental Fig. S2E), and embryos at the two-cell, four-cell, and eight-cell stages showed positive signals of H3K27ac, H3K27me3, and H3K9me3 (Supplemental Fig. S2F). Taken together, these data suggest that histone modifications are largely and globally erased before ZGA, but some histone modifications (H3K27ac, H3K27me3, and H3K9me3) might escape from complete erasure. Hereafter, we referred to them as "retained modifications."

Quantitative ChIP-seq reveals both complete erasure and retention of histone modifications during reprogramming in medaka embryos

Immunofluorescence staining is not only nonquantitative, especially in the case of different nucleus size as observed in medaka embryos (e.g., the 16-cell stage vs. the late blastula stage) (Fig. 1B; Supplemental Fig. S1), but also does not provide reprogramming dynamics at each genomic region. For this reason, conventional ChIP-seq is frequently used to examine the enrichment of histone modifications at specific genomic loci, but it does not allow comparison of the accumulation levels of modifications between samples caused by the lack of normalization of samples (Bonhoure et al. 2014), that is, among different developmental stages (Li et al. 2014). We thus performed quantitative ChIP-seq or "spike-in" ChIP-seq (Bonhoure et al. 2014; Li et al. 2014; Orlando et al. 2014) to investigate the relative amount of each histone modification along the genome among different developmental stages in medaka. We prepared internal reference (or spike-in) chromatin from zebrafish fibroblast cells (BRF41) and mixed it with experimental chromatin (medaka embryo chromatin) in the same tube, which was then subjected to ChIP-seq (Supplemental Fig. S3). Sequenced reads were aligned to the medaka and zebrafish concatenated genome (Supplemental Fig. S3). Theoretically, the accumulation levels of modifications in the reference chromatin should be the same in all samples, so that the

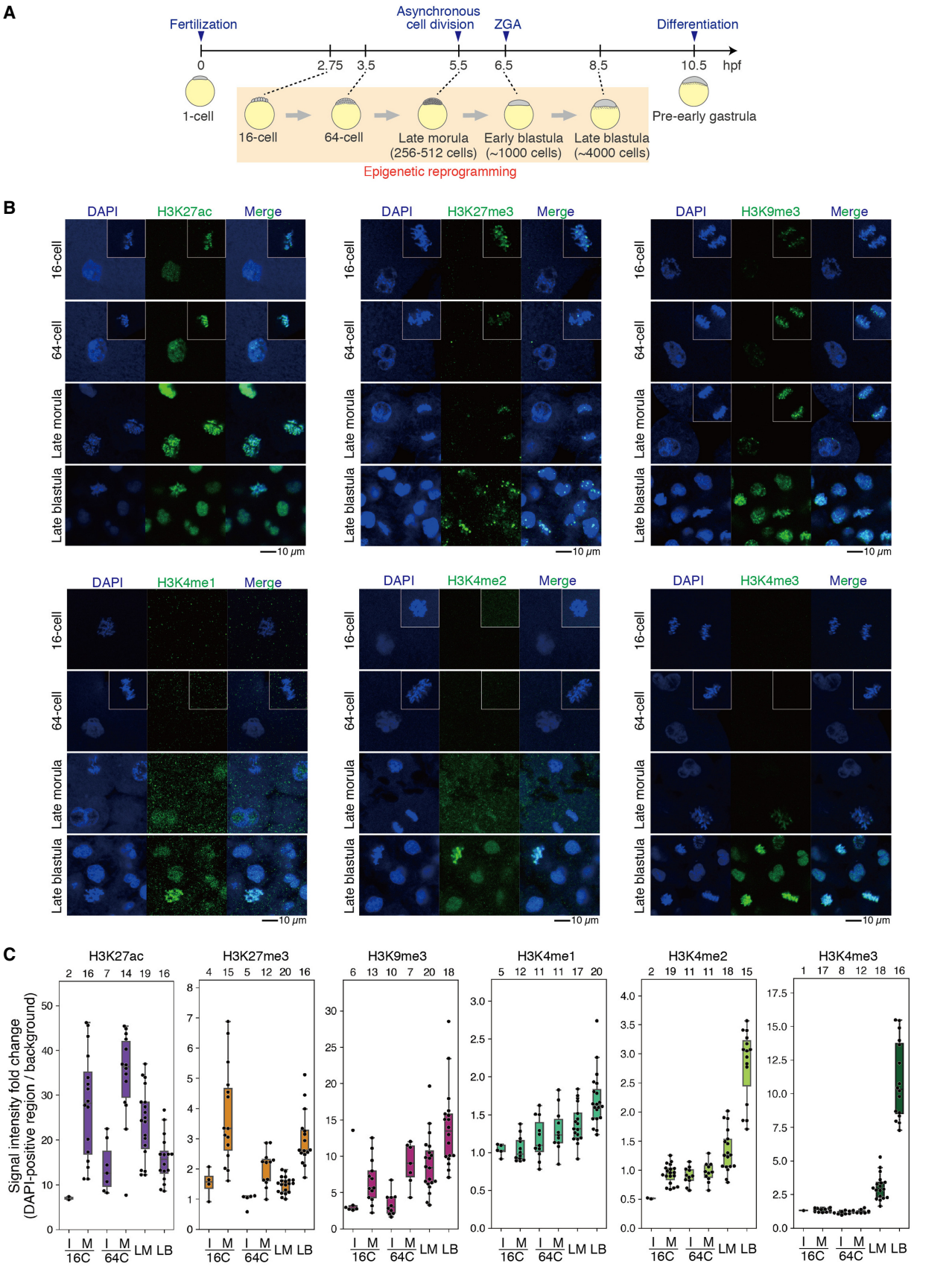

Figure 1. Erasure and retention of histone modifications before ZGA in medaka embryos shown by immunofluorescence staining. (*A*) A schematic of medaka development. (*B*) Immunofluorescence staining of medaka embryos at four stages. The nuclei during mitosis from other embryos are inserted in white boxes. The scale bar indicates 10 μm. (*C*) Boxplots showing the signal intensities of each histone modification in DAPI-positive regions. Each dot indicates the average intensity of 1–3, 3–5, ~40, or ~100 cells in a single broad field slice image of 16-cell (16C), 64-cell (64C), late morula (LM), or late blastula (LB) embryo, respectively. The intensity was normalized by background intensity. Interphase (I) and mitotic phase (M) embryos at the 16-cell and 64-cell stages are separately shown. Phases of cell cycle after the late morula stage are not shown because cells divide asynchronously and are mostly in interphase from the late morula stage. The number *above* each plot shows the number of embryos examined here.

level of histone modifications in medaka chromatin (experimental chromatin) could be normalized using the zebrafish chromatin (reference chromatin) ChIP signal (Supplemental Fig. S3, see also Methods). We confirmed that the reference chromatin ChIP-seq pattern was reproducible for all samples (Supplemental Fig. S4), and spike-in normalization improved the reproducibility of experimental chromatin between two biological replicates, as previously reported (Supplemental Fig. S5A; Bonhoure et al. 2014). We noted that sometimes the correlation between replicates was relatively low (Supplemental Fig. S5A, H3K4 methylations at the 16-cell and 64-cell stages), but that those samples were derived from stages when histone modifications were poorly detected by immunofluorescence staining. In addition, the results of late blastula embryos were very similar to our published data (Supplemental Fig. S5B; Nakamura et al. 2014). Furthermore, the distribution tendency of spike-in ChIP-seq peaks in the medaka genome is largely consistent with that in other vertebrates (Supplemental Fig. S5C; Barski et al. 2007; Zhou et al. 2011). For example, three-quarters of the H3K4me2 and H3K4me3 peaks are located in promoters, whereas the heterochromatin mark H3K9me3 tends to be enriched in gene bodies and intergenic regions (Supplemental Fig. S5C). On the other hand, ChIP-seq using IgG as a negative control and input chromatin did not show any specific accumulations (Figs. 2A, 3A). These data indicate that our "spike-in" ChIP-seq signals of histone modifications are reproducible and specific. We note that our data showed the substantial accumulation of H3K9me3 in promoters and exons in medaka, compared to previous data in zebrafish (Supplemental Fig. S5C,D; Laue et al. 2019). This difference could be attributed to differences in genome size and/or content of transposable elements (Shao et al. 2019).

We first confirmed that dynamics of global histone modification levels in medaka embryos calculated using spike-in ChIP-seq data (see Methods) were similar to those obtained by immunofluorescence staining (Supplemental Fig. S6A). We then asked how the pattern of each modification in the genome is reprogrammed by calculating normalized enrichment levels (termed RPKMspike) (see Methods) (Figs. 2A,B). H3K27ac accumulation was detected and showed similar patterns at all stages examined and its levels gradually increased from the 64-cell stage onward, indicating that both retention and addition of these modifications indeed take place (Fig. 2A,B). H3K27me3 also showed dynamics similar to H3K27ac, but erasure was more intensive (Fig. 2A,B). On the other hands, H3K4 methylation was almost undetectable before the late morula, suggesting its complete clearance (Fig. 2A,B). H3K9me3, the heterochromatin mark, also showed global erasure for most regions but was retained at specific genomic regions (described later) (Fig. 2A,B). We note a slight difference between immunofluorescence staining and spike-in ChIP-seq: H3K4me1 accumulation was low but detected by ChIP-seq at the 16-cell stage (Fig. 2A,B), whereas not by immunofluorescence staining (Fig. 1A, B). This could be caused by the technical limitation of immunofluorescence staining against samples with different nuclear size. In summary, spike-in ChIP-seq revealed that most histone modifications undergo erasure at early stages, albeit to varying degrees, and that H3K27ac, H3K27me3, and H3K9me3 are not completely cleared during epigenetic reprogramming.

It was reported that H3K4me3 primes gene promoters before ZGA in zebrafish (Lindeman et al. 2011). Similarly, our data before spike-in normalization showed the accumulation of H3K4me3 at some promoters in medaka before ZGA (at the late morula stage) (Supplemental Fig. S7A). However, the accumulation levels of those modifications before ZGA were found to be much lower than that after ZGA (at the late blastula stage) by spike-in normalization (Supplemental Fig. S7A,B), suggesting that priming of H3K4 methylation before ZGA is a rare event in medaka. Only H3K27ac showed comparable levels of accumulation before and after ZGA (Fig. 2A,B). Therefore, these data indicate the importance of quantitative normalization of ChIP-seq and raise the possibility of a specific role of H3K27ac retention.

Expression of writers and erasers of histone modifications

The two different dynamics of histone modification reprogramming—complete erasure and residual retention—led us to ask what molecular mechanism underlies this difference. In human embryos, H3K27me3 is globally lost after fertilization, but the same does not occur in mouse embryos. This is thought to correlate with the fact that Polycomb repressive complex 2 (PRC2, a writer and reader complex of H3K27me3) core components, EED and SUZ12, are absent in pre-ZGA human embryos, whereas they are present in pre-ZGA mouse embryos (Xia et al. 2019). We thus reanalyzed the expression levels of writers, erasers, and related proteins of all histone modifications using our published RNA-seq data (Ichikawa et al. 2017; Nakamura et al. 2021), and confirmed their presence (at least, mRNAs) at all stages examined (Supplemental Fig. S8A–E). Therefore, the presence of mRNAs cannot simply explain the lack or abundance of histone modifications in medaka embryos although we do not know the levels of their translated and activated proteins.

H3K9me3 at telomeric regions escapes reprogramming

Although the above spike-in ChIP-seq analysis showed extensive erasure of H3K9me3 at most genomic regions (Fig. 2A,B), immunofluorescence staining detected weak H3K9me3 signals in early-stage embryos (Fig. 1B,C). We thus investigated in what specific regions of the genome H3K9me3 was accumulating at early stages. Closer scrutiny of ChIP-seq tracks revealed that H3K9me3 was broadly and moderately enriched at chromosome ends at all embryonic stages (Fig. 3A,B; Supplemental Fig. S9A), although these regions were not called by the conventional peak calling method. This enrichment was observed in most medaka chromosomes (Supplemental Fig. S9B). In vertebrates, telomeres are located at the ends of chromosomes, and characterized by the absence of genes and enrichment of TTAGGG repeats. The regions adjacent of telomeres are called subtelomeres and characterized by low gene density and enrichment of repetitive sequences (Blasco 2007). Because H3K9me3 is known to accumulate at both telomeres and subtelomeres in somatic cell lines in mouse (García-Cao et al. 2004; Gonzalo et al. 2006), and mainly at subtelomeres in human fibroblasts (Rosenfeld et al. 2009), we hypothesized that H3K9me3 detected at subtelomeres and/or telomeres exceptionally escaped erasure in early-stage medaka embryos. We note that neither IgG nor input chromatin showed the broad and moderate accumulation at chromosome ends in the 16-cell stage (Fig. 3A). Furthermore, we aligned previous zebrafish H3K9me3 ChIP-seq reads (Laue et al. 2019) to medaka genome, but only very limited reads (<0.2%) were aligned to medaka genome (Supplemental Table S5), and there was no specific accumulation at chromosome ends (Supplemental Fig. S9C). Taken together, these data support that H3K9me3 accumulation at chromosome ends observed in ChIP-seq was not caused by the misalignment of zebrafish repeat sequences.

During the mitotic phase, telomeres are found at the ends of chromosome arms of separated chromatids (Ohta et al. 2011).

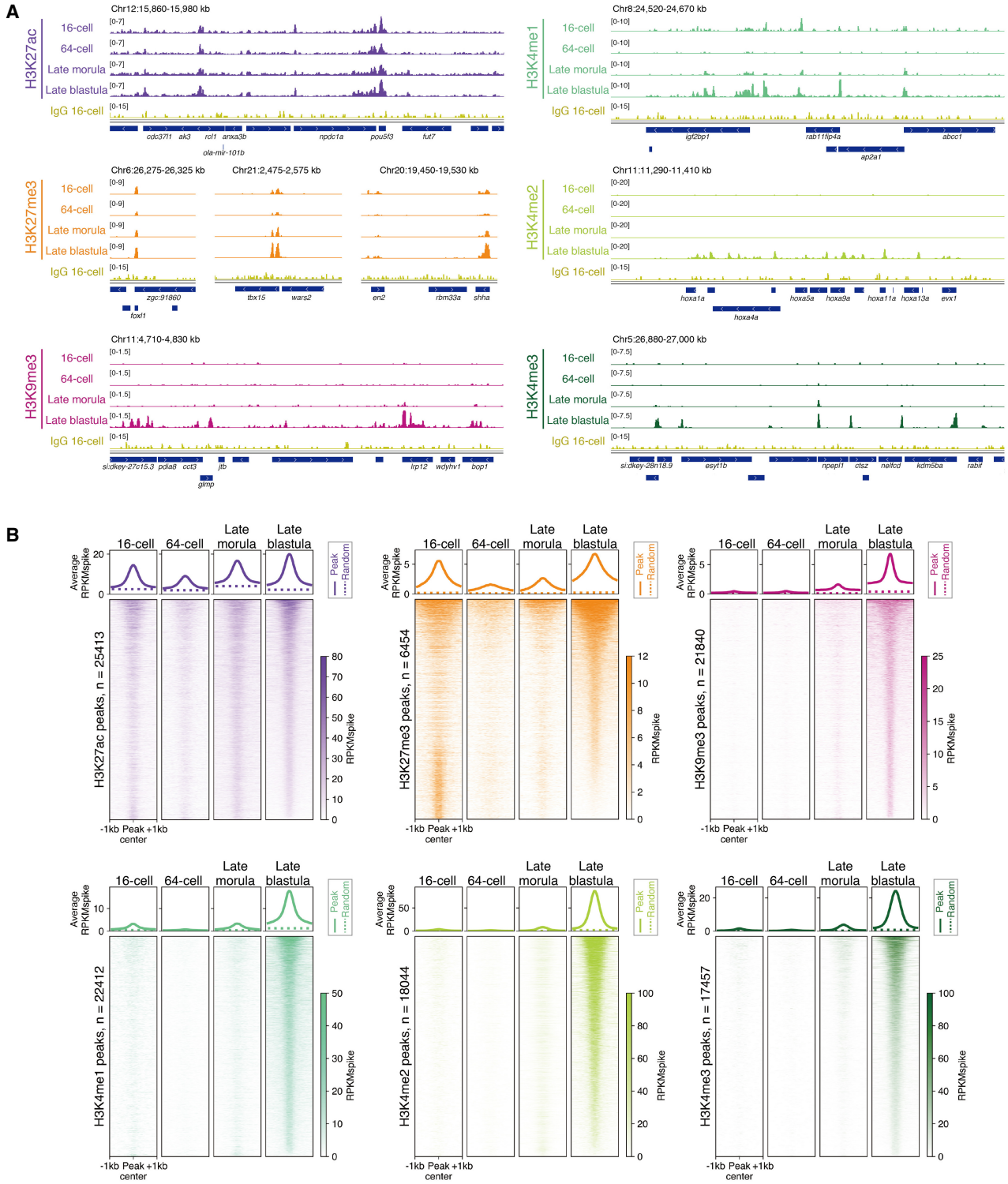

Figure 2. Erasure and retention of histone modifications in early-stage medaka embryos quantitatively revealed by spike-in ChIP-seq. (*A*) Track views showing representative patterns of each histone modification and IgG control. Enrichment levels of histone modifications after spike-in normalization or that of IgG before spike-in normalization are shown. (*B*) Genome-wide changes in enrichment of each modification. The average enrichment levels after spike-in normalization (RPKMspike) around all peaks and randomized peaks at each stage are shown as solid lines and dashed lines, respectively (*top*). Heatmaps showing enrichment levels (RPKMspike) around all peaks (±1 kb from peak center).

Thus, we reanalyzed in detail the immunofluorescence data of H3K9me3 staining at the mitotic phase, and found that the H3K9me3 signals tended to locate at chromosome ends during anaphase (Fig. 3C; Supplemental Fig. S10A). This was also observed in immunofluorescence staining using the other H3K9me3 antibody, whereas not in IgG immunofluorescence staining (Supplemental Fig. S10B). To further confirm the specific localization of H3K9me3 at telomeres and/or subtelomeres, we examined the colocalization of telomere repeats and H3K9me3 signals. For this, we performed fluorescent in situ hybridization (FISH) using probes targeting telomere repeats, followed by immunofluorescence staining of histone modifications, using mitotic chromosomes from 64-cell-stage medaka embryos. As expected, whereas histone H3 signal was globally distributed over whole chromosomes, H3K9me3 signal overlapped with telomeres (Fig. 3D; Supplemental Fig. S10C,D). Because only a few chromosomes have telomere repeats in the current medaka genome assembly (Ichikawa et al. 2017), the H3K9me3-enriched regions at chromosome ends detected by ChIP-seq are likely to be subtelomeres. However, because of the limitation of resolution (Fig. 3D; Supplemental Fig. S10C), we cannot further distinguish telomeres and subtelomeres, and hereafter we simply referred to them as "telomeric regions." Pericentromeres are also known to exhibit H3K9me3 deposition (Dunleavy et al. 2005). However, in medaka, H3K9me3 did not appear to accumulate at pericentromeres at early stages (Fig. 3A). Taken together, these observations show that H3K9me3 escapes reprogramming in early medaka embryos exclusively at telomeric regions.

Removal of H3K9me3 increases genomic instability before ZGA

Next, we addressed the biological significance of H3K9me3 retention at telomeric regions during reprogramming of medaka embryos. We depleted H3K9me3 from early-stage embryos by overexpression of human H3K9me3 demethylase *KDM4D* (hsKDM4D) and examined its effect (Fig. 4A). We first confirmed that overexpression of hsKDM4D greatly reduced the H3K9me3 signals from the 64-cell stage to the late blastula stage both in mitotic cells and interphase cells (Fig. 4B; Supplemental Fig. S11A–C), without affecting the proportion of mitotic cells (Supplemental Fig. S11D). Injected embryos showed impaired gastrulation and severe malformation (Supplemental Fig. S11E,F). We found at earlier stages that H3K9me3 depletion increased the proportion of embryos that showed abnormal chromosome segregation represented by misaligned chromosomes, lagging chromosomes, DNA-bridge formation, and fusion of nuclei, whereas control embryos without injection or injected with a catalytically inactive mutant hsKDM4D(H192A) did not show such tendency (Fig. 4C, D; Supplemental Fig. S11G). Importantly, the increased rate in chromosome-segregation error was observed even at the 64-cell stage, when H3K9me3 accumulates only at telomeric regions in normal embryos (Fig. 3A–D). These data suggest that the residual H3K9me3 at telomeric regions is required for maintenance of chromosome stability during cleavage stages.

H3K27ac premarks active and poised promoters

In contrast to the restricted accumulation of H3K9me3 at telomeric regions, H3K27ac marks were globally deposited at promoters and enhancers at all stages examined (Fig. 2A; Supplemental Fig. S12A). To investigate the developmental changes in H3K27ac accumulation, we first grouped H3K27ac-marked promoters (n = 12,015) into five clusters (Fig. 5A–C; Supplemental Fig. S12B,C; see Methods). In cluster 1, 2, and 3, H3K27ac was accumulated at the 16-cell stage, then its levels decreased at the 64-cell stage, and increased again from the late morula stage onwards (Fig. 5A–C). The dynamics were similar to each other, but the enrichment level was different among these three clusters: cluster 1, "premarked, high"; cluster 2, "premarked, middle"; and cluster 3, "premarked, low," according to their levels at the 16-cell stage. Cluster 4 also exhibits a similar tendency until the late morula stage, but H3K27ac decreased again at the late blastula stage (termed "premarked, decreasing") (Fig. 5A–C). Only cluster 5 promoters did not possess H3K27ac at early stages, and H3K27ac started to accumulate from the late morula stage ("Late H3K27 acetylation") (Fig. 5A–C).

Cluster 4 was unique in that H3K27me3 accumulation levels increased at the late blastula stage whereas H3K27ac decreased (Fig. 5A–C; Supplemental Fig. S13A). H3K4me2 and H3K4me3 also accumulated at the promoters in cluster 4 from the late blastula stage, thus they are poised promoters (Zhou et al. 2011). Importantly, the reciprocal change in H3K27ac and H3K27me3 was more evident after the onset of differentiation (at the pre-early gastrula stage) in cluster 4 (Supplemental Fig. S13A). Gene Ontology (GO) analysis showed that enrichment of terms in cluster 4 is related to developmental genes and transcription factors, which are known targets of PRC2 (Supplemental Fig. S13C). These findings are consistent with the previously described antagonism between H3K27ac and H3K27me3 (Tie et al. 2009) and the switch from H3K27ac to H3K27me3 at developmental gene promoters on ZGA in zebrafish (Zhang et al. 2018a). Taken together, these data suggest that, in cluster 4, the induction of silencing mediated by H3K27me3 proceeds after ZGA.

Inhibition of Crebbp/Ep300 from cleavage stages attenuates accumulation of H3K4 methylation at CpG-dense promoters in the late blastula embryos

We then addressed the functional role of H3K27ac premarking at promoters in early-stage embryos. Importantly, H3K27ac premarking is well correlated with the accumulation of H3K4 methylation at the late blastula, that is, just after ZGA (Fig. 5A–C; Supplemental Fig. S13A,B). Moreover, the analysis of our published ATAC-seq data (assay for transposase accessible chromatin followed by high-throughput sequencing) (Nakamura et al. 2021) showed that the promoters premarked by H3K27ac (clusters 1–4) become accessible earlier than those without H3K27ac premarking (cluster 5); the promoters of clusters 1–4 tended to be open at the early blastula stage and those of cluster 5 become accessible at the late blastula stage (Fig. 5A,B,D; Supplemental Fig. S13B). As described above, the switch from H3K27ac to H3K27me3 occurs in cluster 4 promoters (Fig. 5A–C; Supplemental Fig. S13A). Taken together, these observations raised the possibility that H3K27ac premarking in promoters at early stages contributes to a later gain of accessibility and subsequent accumulation of H3K4 methylation (in clusters 1–4) and H3K27me3 (in cluster 4). Among H3K4 methylation types, we hereafter focus on H3K4me2, because H3K27ac premarking at the 16-cell stage most highly correlated with H3K4me2 after ZGA (the late blastula stage) (Supplemental Fig. S13A,B). As for enhancers, the correlation between H3K27ac premarking and rapid gain of H3K4me2 or chromatin accessibility was not so evident (Supplemental Figs. S14A–C, S15A,B).

To examine if histone acetylation is required for the later establishment of H3K4me2, H3K27me3 deposition, and chromatin

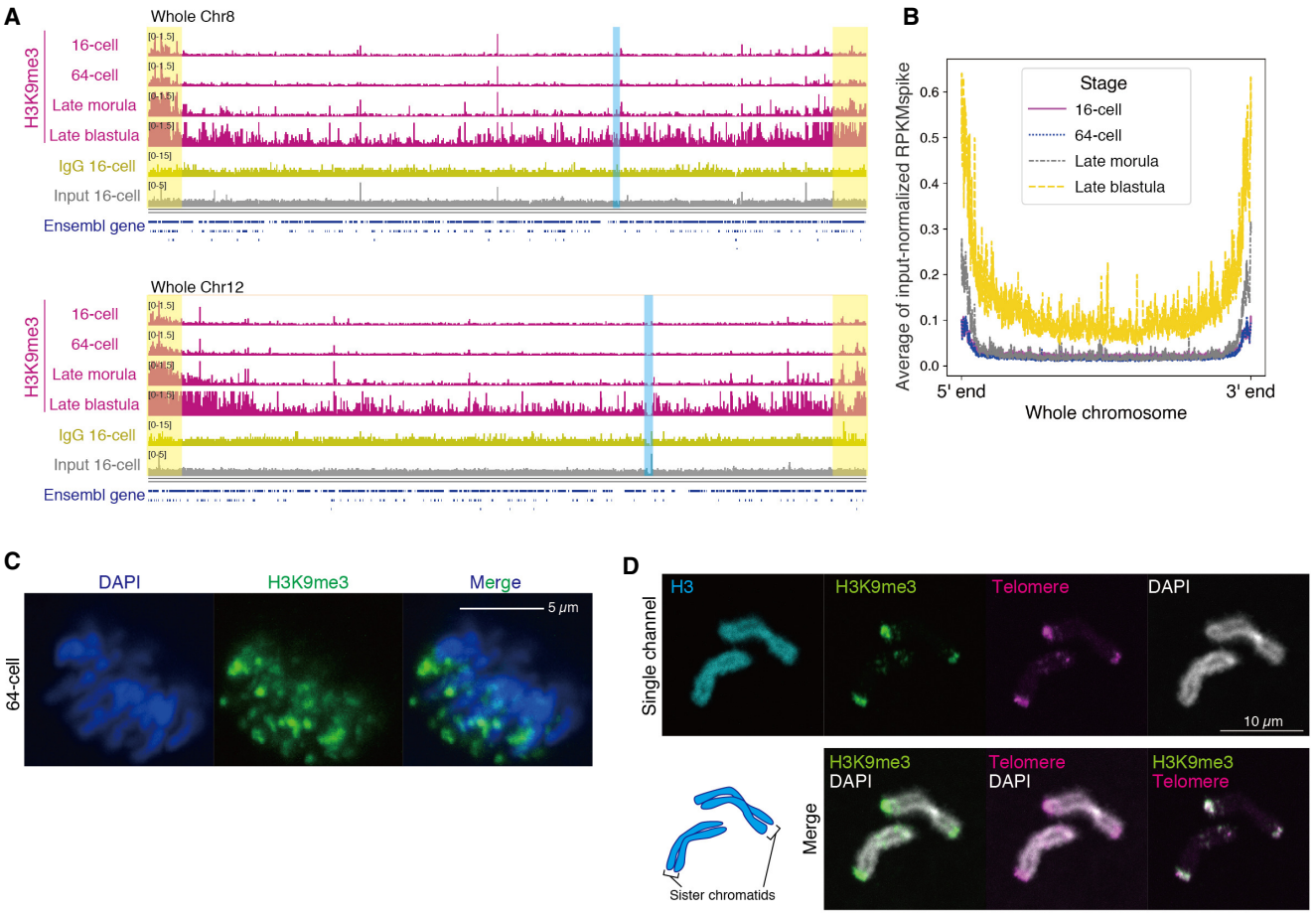

Figure 3. H3K9me3 at telomeric regions escapes reprogramming. (*A*) Track views showing H3K9me3, IgG, and input patterns on representative chromosomes. Whole Chromosome 8 and Chromosome 12 are shown. Ensembl genes are indicated as blue bars. Chromosome ends and centromere positions are highlighted in yellow and blue, respectively. (*B*) Average H3K9me3 signals on all chromosomes at four stages. To exclude the repeat bias, the signal was subjected to spike-in normalization and further normalized by input signal (see Methods). (*C*) Immunofluorescence staining of H3K9me3 during the mitotic phase (anaphase) at the 64-cell stage. (*D*) FISH and immunofluorescence staining using chromosome spreads from embryos at the 64-cell stage. Sister chromatids are shown as representatives.

accessibility at promoters, we treated embryos with the A485, a specific and catalytic inhibitor of Crebbp/Ep300 (Lasko et al. 2017; Hogg et al. 2021; Narita et al. 2021; Pelham-Webb et al. 2021). When embryos were incubated with A485 from the two-cell stage, the H3K27ac level was globally reduced as shown by immunofluorescence staining (Supplemental Fig. S16A,B). This treatment drastically impaired gastrulation (Supplemental Fig. S16C, D), consistent with a previous study showing gastrulation arrest after global H3K27ac reduction in zebrafish (Chan et al. 2019). In addition, in line with previous zebrafish studies (Zhang et al. 2018a; Chan et al. 2019), the inhibition of Crebbp/Ep300 impaired ZGA in medaka (Supplemental Fig. S18F).

Next, the effects of Crebbp/Ep300 inhibition were examined by spike-in ChIP-seq using DMSO- or A485-treated late blastula embryos. After validating the reproducibility of experiments (Supplemental Fig. S17A), we first confirmed that the global H3K27ac level was significantly reduced after A485 treatment (Fig. 6A,B). We next compared the H3K4me2 levels at H3K27ac promoter peaks, and found that about 16% of H3K27ac promoter peaks showed significant reduction in H3K4me2 level after A485 treatment ("H3K4me2 down," n = 1578 vs. "H3K4me2 nonsensitive," n = 8344 in Fig. 6A,B).

We then sought to identify certain genetic and/or epigenetic factors which could explain the sensitivity of H3K4me2 to the loss of H3K27ac. Based on the aforementioned correlation between H3K27ac, H3K4me2, and H3K27me3 at some promoters in normal development (cluster 4 in Fig. 5A–C), we first compared H3K27me3 levels at H3K27ac peaks. However, only a portion (19.6%) of "H3K4me2 down" peaks showed an increase in H3K27me3 level ("H3K4me2 down H3K27me3 up," n = 309) (Fig. 6A,B; Supplemental Fig. S17B), suggesting that the gain of H3K27me3 alone cannot explain the sensitivity of H3K4me2 to A485 treatment. We next focused on CpG density and DNA methylation, because the H3K4 methylation writer complexes COMPASS and COMPASS-like are known to bind to hypomethylated CpGs (Macrae et al. 2022). We found that the CpG densities of "H3K4me2 down" and "H3K4me2 down H3K27me3 up" peaks were significantly higher than those of "H3K4me2 nonsensitive" peaks (Fig. 6C; Supplemental Fig. S17C–E). On the other hand, reanalysis of DNA methylation in normal blastula embryos (Qu et al. 2012) revealed that DNA methylation levels in both "H3K4me2 down" and "H3K4me2 nonsensitive" peaks were almost comparably low, excluding the possibility that original DNA methylation levels affect the sensitivity of H3K4me2 to the loss of histone

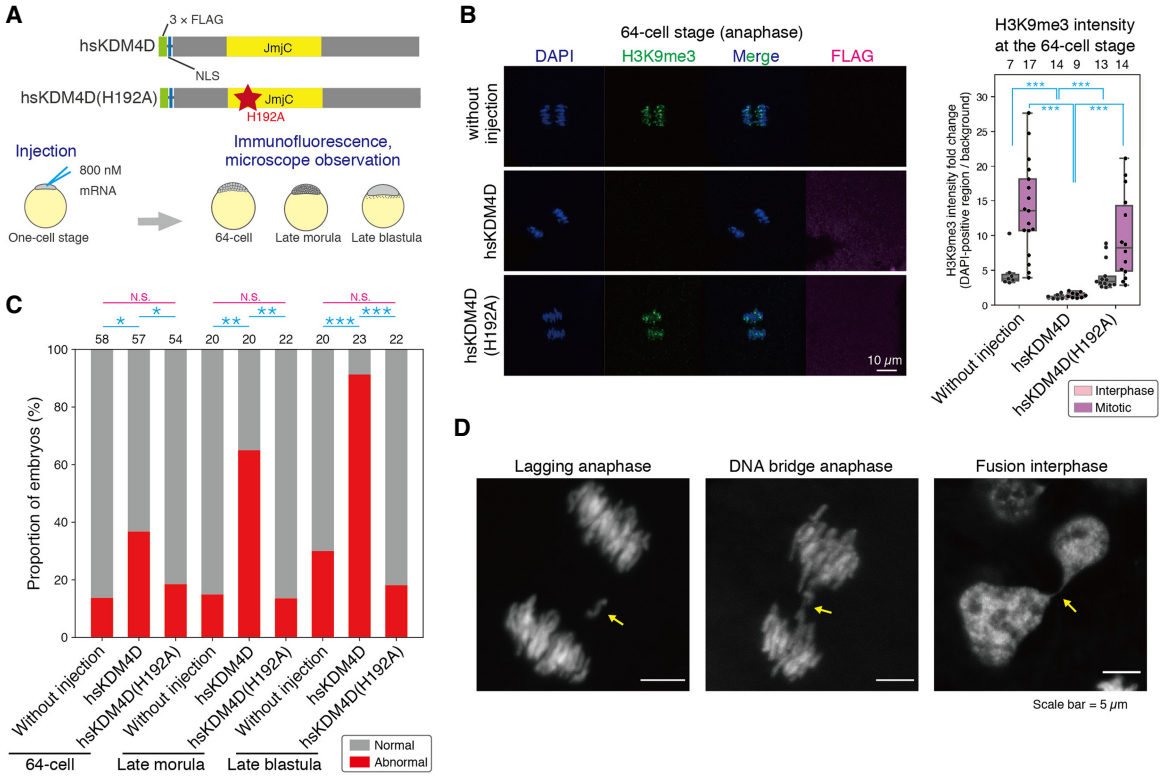

Figure 4. Removal of H3K9me3 increases genomic instability before ZGA. (*A*) Schematic illustrations of hsKDM4D constructs (wild-type hsKDM4D and its catalytically inactive point mutant hsKDM4D(H192A)) and experimental design. (*B*) Immunofluorescence staining of H3K9me3 during the mitotic phase (anaphase) at the 64-cell stage after injection of hsKDM4D or hsKDM4D(H192A) and its quantification. Boxplots showing the signal intensities of each histone modification in DAPI-positive regions. Each dot indicates the average intensity of 3–5 cells in a single broad field slice image of 64-cell embryo. The intensity was normalized by background intensity. The number *above* each plot indicates the number of embryos examined. Dwass, Steel, Critchlow, and Fligner all-pairs comparison test was performed. (*C*) Percentage of embryos having abnormal chromosome segregation phenotypes. The number *above* each bar shows the number of embryos examined in each condition. Two-sided Fisher's exact test was performed and *P*-values were normalized by the Holm method. (*D*) Representative phenotypes of chromosome segregation errors. Arrows indicate the error. (***) $P<0.001$, (**) $P<0.01$, (*) $P<0.05$, respectively.

acetylation (Supplemental Fig. S17C,D). Taken together, these results suggest that H3K4me2 at CpG-dense promoters is vulnerable to the inhibition of Crebbp/Ep300 (Supplemental Fig. S20C).

Next, we examined chromatin accessibility at the late blastula stage by performing ATAC-seq using DMSO- or A485-treated late blastula embryos. After validating the reproducibility and quality of ATAC-seq (Supplemental Fig. S18A,B), we found that global reduction of H3K27ac had only minor effects on the ATAC-seq pattern at the late blastula stage ("ATAC nonsensitive" = 6234, "ATAC up" = 16, "ATAC down" = 24) (Fig. 6A,D). Although some H3K27ac peaks were associated with reduced chromatin accessibility after A485 treatment (Fig. 6A; Supplemental Fig. S18C), the number of such changes were very limited (Supplemental Fig. S18D). Consistently, recent studies in zebrafish embryos, mouse embryonic stem cells, and a human cell line revealed that H3K27ac is dispensable for chromatin opening (Martire et al. 2019; Hunt et al. 2022; Miao et al. 2022). Therefore, we concluded that the gain of chromatin accessibility at the late blastula stage is largely independent of H3K27ac accumulation.

Finally, we assessed the specificity of the effect of A485 treatment on H3K4me2. First, we found that a reduction in H3K4me2 occurred exclusively within H3K27ac peaks; the number of regions where H3K4me2 level was reduced was 1040 in the H3K27ac-positive regions, whereas only 160 in the H3K27ac-negative regions (Supplemental Fig. S18E). Second, none of the genes directly involved in deposition and erasure of H3K4me2 or H3K27me3 showed significant changes in expression levels after A485 treatment (Supplemental Fig. S18F,G). Third, H3K4me2 accumulated to comparable levels to normal embryos at the majority of promoters in A485-treated embryos (Fig. 6A,B). These data suggest that the dysregulations of H3K4me2 and H3K27me3 in A485-treated embryos were not caused by improper gene expressions or developmental delay.

For technical reasons, we were unable to deplete H3K27ac specifically and transiently before the late blastula stage, and thus we could not distinguish between the requirement of premarking before ZGA or H3K27ac at the late blastula stage. Nevertheless, our data suggest that Crebbp/Ep300 induces H3K27ac premarking and that its activity is required for proper accumulation of H3K4me2 at CpG-dense promoters, but is dispensable for the gain of chromatin accessibility at the late blastula stage.

Polycomb high-affinity regions escape complete erasure of H3K27me3 during reprogramming

We found weak retention of H3K27me3 at specific sites during reprogramming, although H3K27me3 is extensively erased throughout the genome (Fig. 2A,B). We classified the H3K27me3 marked

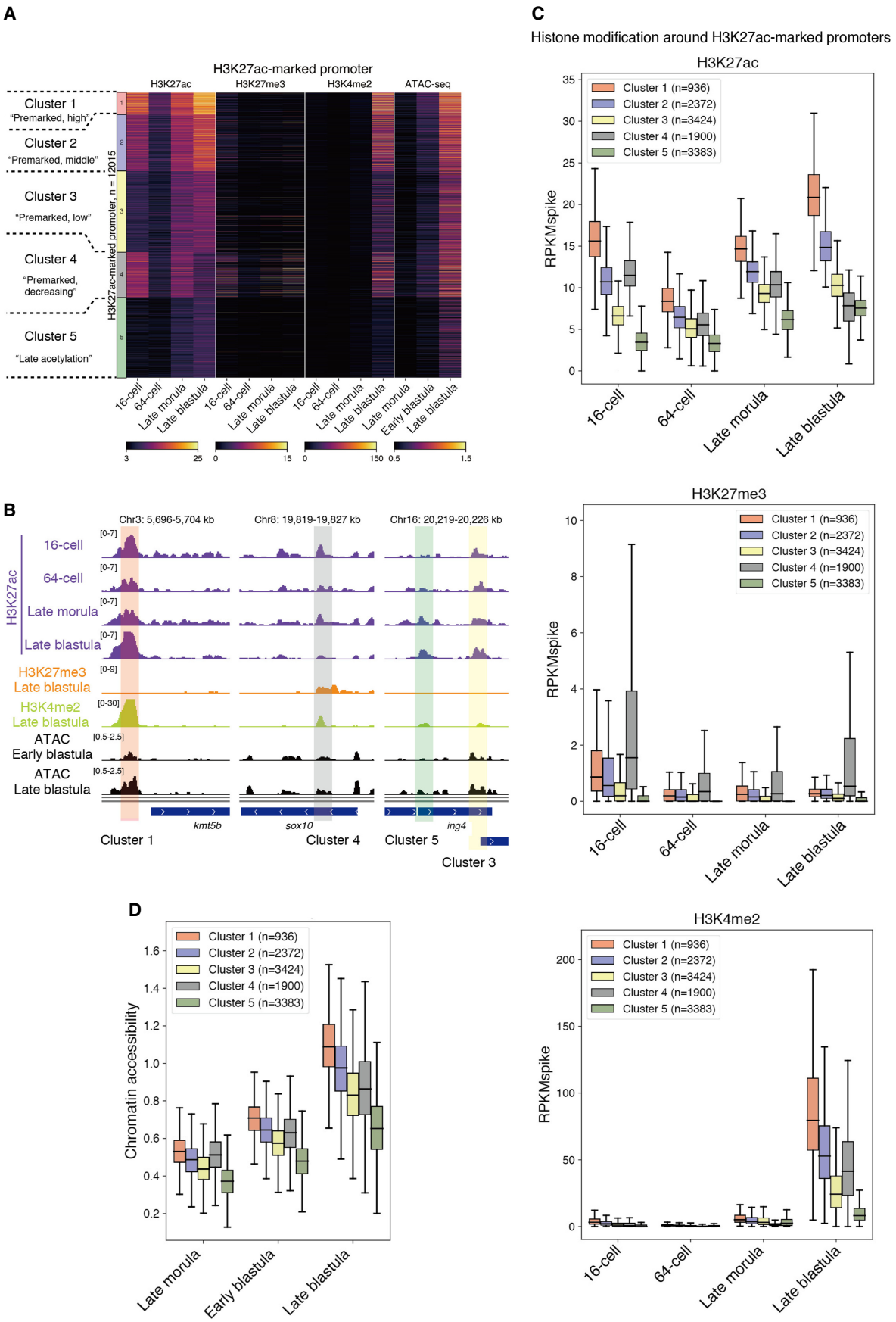

Figure 5. H3K27ac premarking is associated with future gain of histone modifications and accessibility at later stages in medaka. (*A*) Heatmap showing histone modification enrichments (H3K27ac, H3K27me3, and H3K4me2) and chromatin accessibility (Nakamura et al. 2021) at H3K27ac-marked promoter peaks after clustering. (*B*) Track views of examples of H3K27ac-marked promoter peaks. The histone modification enrichments after spike-in normalization and chromatin accessibility are shown. Peaks from different clusters are highlighted using different colors. (*C*) Boxplots showing histone modification levels after spike-in normalization (RPKMspike) in each H3K27ac-marked promoter cluster. The outliers are not shown. (*D*) Boxplots showing chromatin accessibility around H3K27ac-marked promoters in each cluster.

regions into three groups ("Erasure," "Low retention," and "Mild retention") by the accumulation levels of H3K27me3 at the 64-cell stage, a stage when H3K27me3 enrichment was at the lowest level during reprogramming (Supplemental Fig. S19A). We found that the retained region is associated with the following genetic and epigenetic features of Polycomb high-affinity sequences: (i) high CpG density (Ku et al. 2008; Mendenhall et al. 2010; van Mierlo et al. 2019) and high GCG density (Supplemental Fig. S19B; Perino et al. 2018, 2020); (ii) DNA hypomethylation (Nakamura et al. 2014) at the blastula stage (Supplemental Fig. S19C; Qu et al. 2012); (iii) transcription factors and genes related to developmental processes such as Homeobox (Supplemental Fig. S19D–F; Schuettengruber et al. 2017). Importantly, the analysis of maternally derived transcripts showed that the genes with mild retention are more strongly suppressed in oocytes (Supplemental Fig. S19G), suggesting maternal inheritance of H3K27me3 like in mouse (Inoue et al. 2017), in *Drosophila* (Zenk et al. 2017), and in *Arabidopsis thaliana* (Luo et al. 2020).

Discussion

Reprogramming of epigenetic modification is a critical process during early development. However, the dynamics of histone modification reprogramming and the function of retained modifications had not been fully understood in vertebrates. Here, our genome-wide and time-course quantitative analyses revealed that not all histone modifications are subject to complete erasure in medaka embryos. Among the major histone modifications we examined, H3K4 methylation and H3K9me3 are completely erased during reprogramming but H3K27ac, H3K27me3, and telomeric H3K9me3 are not (Fig. 6E). With this comprehensive and quantitative dataset in hand, we experimentally revealed the essential roles of the retained histone modifications in medaka early development.

The difference between retained modifications and erased modifications

What mechanism determines whether a modification is retained or erased? At present, these differences cannot simply be explained by the lack or abundance of writers and erasers, as transcripts of all of these are present at all stages (Supplemental Fig. S8).

Because new and free histones are incorporated into chromatin during DNA replication (Stewart-Morgan et al. 2020), the rapid cell cycle in fish early development (Fig. 1A; Jukam et al. 2017) accelerates dilution of all histone modifications. This passive erasure could explain the massive reduction of all histone modifications during reprogramming. In contrast, active maintenance should work at least for "retained modifications." In particular, H3K27ac maintains a comparable level of accumulation during epigenetic reprogramming under rapid cell-cycling (Fig. 2A,B), and this may require strong de novo deposition during cleavage stages. Future investigations are warranted to elucidate molecular mechanisms that enable well-balanced erasure and writing of modifications during early development.

H3K9me3 protects telomeres

One of the interesting and novel findings of our study is the retention of H3K9me3 at telomeric regions during early development and its role in chromosome stability during cleavage stages. How is abnormal chromosome segregation induced when telomeric H3K9me3 is removed in early embryos? In general, because of the 3′ overhang of telomere repeats, telomeres can be targeted by DNA damage sensing machinery or DNA repair machinery (O'Sullivan and Karlseder 2010). To avoid this situation, telomeres are protected by a special protein complex called shelterin, and disruption of shelterin complex results in an increase in genomic instability, which is frequently correlated with cancer development (O'Sullivan and Karlseder 2010). Notably, the representative phenotypes caused by the failure of telomere protection (telomere dysfunction) are DNA-bridge formation and fusion of two interphase nuclei (Maciejowski et al. 2015; Umbreit et al. 2020), which are similar to those observed in H3K9me3-depleted embryos in this study (Fig. 4D; Supplemental Fig. S11D). Thus, although we cannot exclude the possibility that a demethylation of nonhistone targets causes the genomic instability in hsKDM4D-overexpressed embryos, our results suggest that the exceptional retention of H3K9me3 at telomeric regions are involved in telomere protection during early development (Supplemental Fig. S20A).

In cultured cells, accumulation of H3K9me3 is broadly observed in heterochromatic regions including telomeres or subtelomeres (García-Cao et al. 2004; Gonzalo et al. 2006; Rosenfeld et al. 2009). A previous study using cultured fibroblast and embryonic stem cells reported that global depletion of H3K9me3, achieved by knocking out H3K9 methyltransferases, resulted in abnormal telomere elongation but did not show telomere dysfunction phenotypes with genome instability observed in our study, such as chromosome fusions (García-Cao et al. 2004). Given that cultured cells are slow-growing, it is possible that cleavage-stage embryos require H3K9me3-dependent telomere protection in addition to a shelterin-mediated one to achieve stable chromosomal segregation in rapid cell-cycling.

The function and molecular mechanisms of H3K27ac premarking

Previous studies showed that H3K27ac accumulates from the four-cell stage in zebrafish embryos (Zhang et al. 2018a), and that inhibition of histone acetyltransferase or acetylation reader disrupted proper ZGA in zebrafish embryos (Zhang et al. 2018a; Chan et al. 2019; Sato et al. 2019). Consistent with these studies, H3K27ac marking is present in medaka embryos before ZGA (Fig. 2A,B). However, there was no experimental data that explains how H3K27ac contributes to the epigenetic landscape during ZGA. In this study, we experimentally showed that Crebbp/Ep300 induces H3K27ac premarking and that its activity is required for proper accumulation of H3K4me2 at CpG-dense promoters (Fig. 6A–D). Our data is largely consistent with a model previously proposed in zebrafish, based on the correlation of histone modification patterns, that H3K27ac at promoters primes the future accumulation of H3K4me3 (Zhang et al. 2018a).

The molecular mechanism underlying the H3K27ac premarking and later gain of H3K4me2 is still unknown. However, it is worth noting that in mammalian cell lines, H3K27ac reader BRD4 was shown to interact with Mediator (Jang et al. 2005), and also that H3K4 methylation writer COMPASS complex is known to interact with Mediator (Quevedo et al. 2019). Furthermore, it was reported that H3K27ac at promoters is recognized by BRD2, another reader of H3K27ac, which in turn mediates H3K4me3 installation and gene activation (Zhao et al. 2021). Thus, induction of H3K4 methylation by H3K27ac in the early medaka embryos may also be mediated by Brd2/4 (Supplemental Fig. S20B). Importantly, our analysis further showed that H3K4me2 at CpG-dense promoters is vulnerable to inhibition of Crebbp/Ep300. We also found that H3K27me3 was increased at a fraction of promoters. CpG islands are subject to

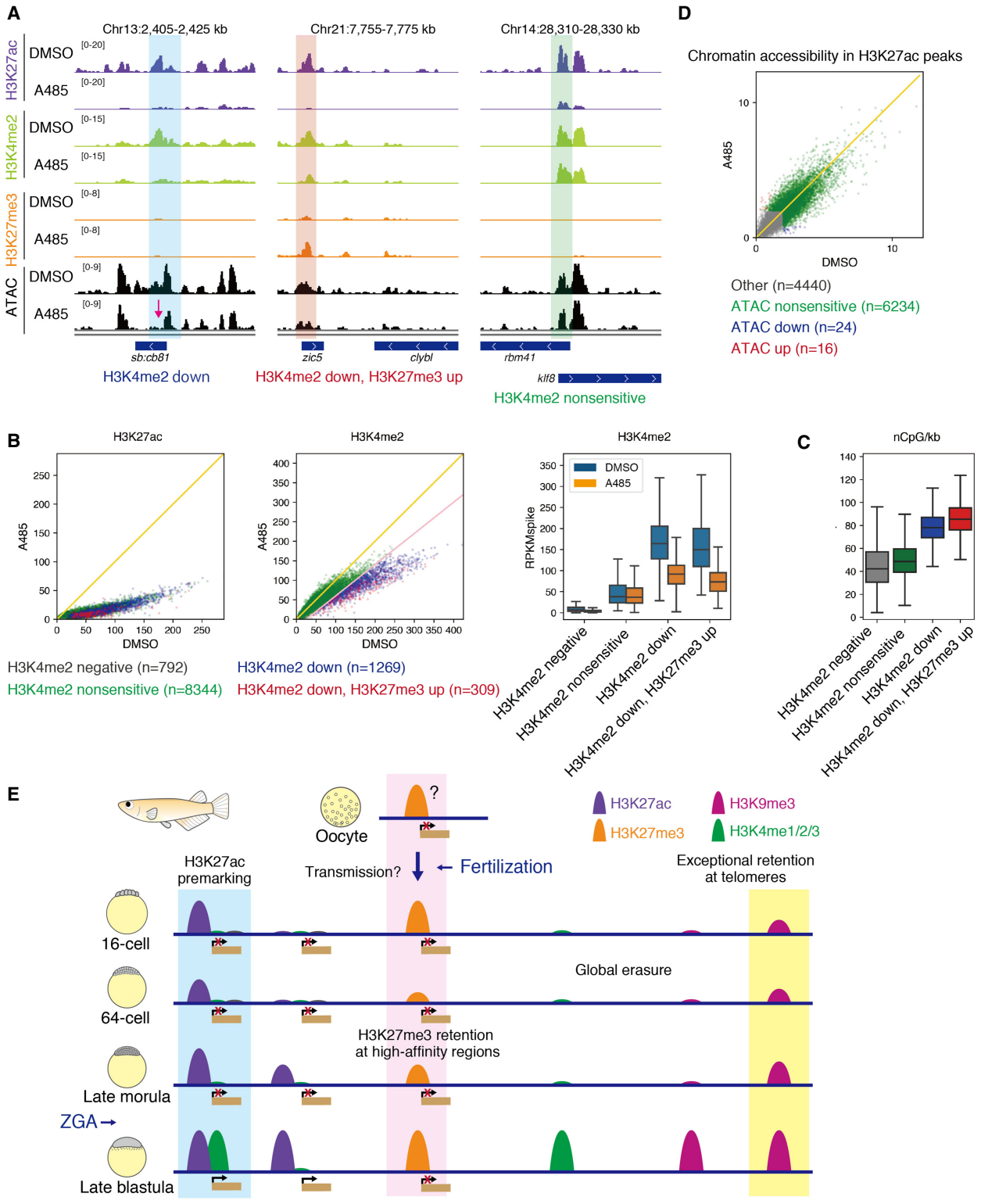

Figure 6. H3K27ac is required for proper histone modification patterning in late blastula embryos. (*A*) Track views showing the histone modification enrichments after spike-in normalization and chromatin accessibility in DMSO- or A485-treated embryos. The magenta arrow indicates where chromatin accessibility was altered after A485 treatment. (*B*) Comparison of H3K27ac enrichment and H3K4me2 enrichment in H3K27ac peaks between A485 and DMSO treatment by scatter plots (*left*) and boxplots (*right*). Yellow and pink lines indicate Y = X and Y = 0.8 × X − 20, respectively. (*C*) Comparison of CpG density (number of CpGs/kb) in H3K27ac peaks between A485 and DMSO treatment by a boxplot (*right*). (*D*) Scatter plot showing chromatin accessibility in H3K27ac peaks in DMSO and A485 treatment. "Other" indicates the H3K27ac peaks with low ATAC-seq signals. Yellow line indicates Y = X. (*E*) Summary of histone modification reprogramming in medaka. All histone modifications more or less undergo erasure after fertilization, but some modifications escape complete erasure in medaka. H3K27ac premarks promoters and is required for proper patterning of histone modification (e.g., H3K4me2). H3K27me3 is probably transmitted maternally and retained at Polycomb high-affinity regions, although the enrichment was very limited. H3K9me3 at telomeric regions escapes complete erasure and is required for maintenance of chromosome stability during cleavage stage. On the other hand, H3K4 methylations and H3K9me3 except at telomeric regions are extensively erased after fertilization.

not only the binding of COMPASS/COMPASS-like but also PRC1/2 (van Mierlo et al. 2019; Macrae et al. 2022), and the antagonistic activity of COMPASS/COMPASS-like and PRC1/2 has been shown (Piunti and Shilatifard 2016; Macrae et al. 2022). Thus, it is likely that H3K27ac serves as a safeguard for accumulation of H3K4me2 after ZGA by impeding PRC1 and/or PRC2 binding at the CpG-dense promoters (Supplemental Fig. S20C). Importantly, it was reported in zebrafish that silencing by PRC1 precedes that of PRC2 around ZGA (Hickey et al. 2022). This may account for our data that only a portion of H3K4me2 reduction correlated with an increased PRC2 activity (i.e., increased H3K27me3 accumulation) (Fig. 6A,B). At the moment, however, we cannot exclude the possibility that other Crebbp/Ep300-dependent histone acetylations such as H3K18ac and H3K36ac (Shvedunova and Akhtar 2022) are also involved in this scenario.

We also showed that the global reduction in H3K27ac by inhibition of Crebbp/Ep300 did not cause loss of chromatin accessibility at promoters (Fig. 6A,D), in spite of the strong correlation between H3K27ac premarking and gain of chromatin accessibility after ZGA (Fig. 5A,B). This is largely consistent with recent studies in zebrafish embryos (Miao et al. 2022), mouse embryonic stem cells (Martire et al. 2019), and a human cell line (Hunt et al. 2022). These facts suggest the presence of a Crebbp/Ep300-independent mechanism to regulate chromatin accessibility such as H2A.Z (Murphy et al. 2020).

Retention of H3K27me3 during reprogramming

Residual H3K27me3 was observed in early medaka embryos (Supplemental Fig. S19A), and genes with H3K27me3 retention were strongly repressed in oocytes (Supplemental Fig. S19G). However, the H3K27me3 level at the 64-cell stage (middle of reprogramming) was much lower than that at later gastrulation stage (Supplemental Fig. S6A,B). Furthermore, unlike mouse and *Drosophila*, loss of maternally supplied H3K27me3 by maternal *ezh2* knockout did not affect zebrafish development as long as *ezh2* was zygotically expressed (Rougeot et al. 2019). Thus, the biological significance of the retained H3K27me3 for later development in teleosts remains unclear.

In summary, the present study quantitatively determined reprogramming dynamics of histone modifications and experimentally showed previously unknown roles of retained histone modifications in early nonmammalian embryos, providing novel insights into epigenetic reprogramming during early embryogenesis.

Methods

Fish strains and handling

In this study, medaka d-rR strain was used for all experiments. Medaka fish were maintained and raised according to standard protocols (Kinoshita et al. 2009). Fertilized embryos were raised under standard protocols (Kinoshita et al. 2009) at 28°C. Developmental stages were determined based on previously published guidelines (Iwamatsu 2004). All experimental procedures and animal care were performed according to the animal ethics committee of the University of Tokyo (Approval No. 20-2).

Cell lines

In this study, BRF41 (zebrafish fibroblast cell line) and HEK293 were used. BRF41 was cultured with L-15 medium supplemented with 15% FBS and 1% Penicillin Streptomycin at 33°C. HEK293 was cultured with DMEM.

Immunofluorescence staining and imaging

Fertilized eggs were manually collected and incubated at 28°C. Medaka embryos at appropriate stages were fixed with 4% PFA/PBS for 4 h at room temperature and overnight at 4°C. After washing and manual dechorionation, embryos were permeabilized with 0.5% Triton X-100/1 × PBS for 30 min, washed with PBS for 5 min at room temperature 3 times, blocked with blocking buffer (2% BSA, 1% DMSO, 0.2% Triton X-100, 1 × PBS) for 1 h at room temperature. The primary antibody (Supplemental Table S1) was added, and samples were incubated at 4°C overnight. Samples were washed with PBSDT (1 × PBS, 1% DMSO, 0.1% Triton X-100) for 15 min 5 times at 4°C, blocked again with blocking buffer at room temperature for 1 h, incubated with blocking buffer including DAPI and secondary antibody (Supplemental Tables S1, S2) for 4 h at 4°C, washed with PBSDT for 15 min at 4°C 5 times, and finally buffer was replaced by PBS. Blastomeres were isolated from yolk and mounted on slide glasses with 50% glycerol/PBS. Imaging was performed using Zeiss LSM710. All imaging data using the same antibody were taken under the same conditions. The images in Figures 3C, 4D, Supplemental Figures S2E, S10A,B, and S11G are the maximum intensity projection of z-stack images, and others are single slice images. Quantifications were performed using Fiji (Supplemental Methods; Schindelin et al. 2012).

Wild-type and catalytically inactive mutant hsKDM4D expression vector cloning

Total RNA from 2 d-post-fertilization medaka embryos and HEK293 were reverse transcribed to cDNA mix using SuperScript III First-Strand Synthesis SuperMix (Invitrogen 18080400) for cloning of olKdm6ba and hsKDM4D, respectively. olKdm6ba was amplified from the cDNA mix using cloning primers (forward: GAGAGAAGAAGGACCGCATG, reverse: TCGGAGAGTCACAGCAGGA). hsKDM4D was amplified from the cDNA mix using cloning primers (forward: GTACGCTGGTAGATCCTGCT, reverse: GCATGCCTAGAGTCCTGCAA). PCR products were cloned into the pCRII-TOPO vector (Invitrogen K465001). The olKdm6ba and hsKDM4D sequences were amplified using primers including 3 × FLAG and NLS sequences, and assembled into BamHI and XhoI-linearized pCS2+ vector using NEBuilder HiFi DNA Assembly Master Mix (NEB E2621). The H377A mutation in olKdm6ba and the H192A mutation in hsKDM4D were induced by PrimeSTAR Mutagenesis Basal Kit (Takara R046A) using the following primer pairs (forward: GCCGGGTGCCCAGGAGAACAATAATTT, reverse: TCCTGGGCACCCGGCGTCCGGCTCCC) and (forward: TGCTTGGGCTACAGAGGACATGGAC, reverse: TCTGTAGCCCAAGCAAACGTGGTT), respectively. The H377A mutation in olKdm6ba corresponds to a catalytically inactive point mutant of mouse *Kdm6b* [Kdm6b(H1390A)] in previous studies (Xiang et al. 2007; Inoue et al. 2017). The H192A mutation in hsKDM4D corresponds to the catalytically inactive point mutant of mouse *Kdm4d* [Kdm4d(H189A)] in a previous study (Matoba et al. 2014).

In vitro transcription

The templates of olKdm6ba, olKdm6ba(H377A), hsKDM4D, and hsKDM4D (H192A) mRNA for in vitro transcription were generated by PCR from pCS2+ vectors using the following primers (forward: TGACGTAAATGGGCGGTAGG, reverse: CAGGAAACAGCTATGAC). mRNA was synthesized using mMESSAGE

mMACHINE SP6 Transcription Kit. RNeasy Mini Kit was used to purify RNAs (Supplemental Table S2).

RNA injection

294 ng/µL (400 nM) of olKdm6ba or olKdm6ba(H377A), or 514 ng/µL (800 nM) of hsKDM4D or hsKDM4D(H192A) mRNAs was injected into one-cell-stage (stage 2) embryos.

Spike-in ChIP-seq library preparation and sequencing

ChIP experiment was performed as previously described (Fukushima et al. 2019) with modifications. Briefly, medaka embryos or zebrafish fibroblast cells were fixed and sonicated independently, assembled into same tube, and incubated overnight with beads-antibody premix (Supplemental Table S1). DNA was purified by phenol: chloroform: isoamyl alcohol method and ethanol purification. ChIP-seq libraries were prepared using KAPA Hyper Prep Kit. All ChIP-seq libraries were sequenced using the Illumina HiSeq 1500 system. Details of the ChIP procedure are in Supplemental Methods.

After sequencing, raw reads were aligned to the medaka (HdrR) and zebrafish (Zv9) concatenated genome, processed as previously described (Fukushima et al. 2019), normalized (spike-in normalization) as previously described (Supplemental Methods; Li et al. 2014). Mapping information is shown in Supplemental Table S4. Peak calling, peak annotation, and Gene Ontology analysis were performed using MACS2 (Zhang et al. 2008), HOMER annotatePeaks.pl (Heinz et al. 2010), and PANTHER (Mi et al. 2019), respectively (Supplemental Methods). *k*-means clustering was performed for H3K27ac peaks (Supplemental Methods). For A485-treatment analysis, the changes in enrichment larger than thresholds were defined as significant ones (Supplemental Methods).

A485 treatment and ATAC-seq

Fertilized eggs were dechorionated and incubated with 20 µM A485 or DMSO (Supplemental Table S2) from the two-cell stage to the late blastula stage. These embryos were used for subsequent immunofluorescence staining, or spike-in ChIP-seq as described above. ATAC-seq using A485-treated or DMSO-treated embryos were conducted as previously described (Nakamura et al. 2021) with modification (Supplemental Methods).

RNA-seq

RNA-seq using A485-treated late blastula embryos was conducted as previously described (Nakamura et al. 2021). Briefly, A485-treated embryos were homogenized in 1 mL of ISOGEN, 200 µL of chloroform was added, and total RNA was purified using RNeasy mini kit. rRNA was depleted using RiboMinus Eukaryote System v2 using 1 µg of total-RNA as input (Supplemental Table S2). After rRNA depletion, RNA-seq libraries were generated using a KAPA RNA HyperPrep kit. All RNA-seq libraries were sequenced using the Illumina HiSeq 1500 system. RNA-seq data were processed as previously described (Nakamura et al. 2021) and FPKM, RPKM, and adjusted *P*-value were generated by R library DESeq2 (Supplemental Methods; Love et al. 2014).

FISH and immunofluorescence of chromosome spreads

Dechorionated embryos were homogenized at the 64-cell stage by pipetting up and down in 1× PBS. After centrifugation, the pellet was dissolved with fixative (1% PFA with 0.2% Triton X-100, pH 9.2), cells were spread on glass slides, and incubated overnight at 4°C in a humid chamber. After washing, hybridization solution (50% formamide, 5× SSC, 50 µg/mL heparin, 500 µg/mL tRNA, 0.1% Tween 20, 1.35 mg/mL BSA, 0.2 µM TelC-Cy3, pH ~6) was placed on a slide. After denaturing at 80°C for 10 min, slides were placed in a humid chamber and incubated at 37°C overnight. The slides were washed, blocked with blocking buffer (same as for immunofluorescence staining), and incubated with primary antibody at 4°C overnight. After washing, slides were incubated with secondary antibody at 37°C for an hour. Finally, slides were washed, VECTASHIELD Mounting Medium with DAPI was added to slides, and coverslips were placed on slides. Imaging was performed using Zeiss LSM710. Fractions of TelC and H3K9me3/H3 particles overlapping with others were calculated using a Fiji plugin, JACoP (Pearson's correlation & Objects based method) (Bolte and Cordelières 2006). The fractions were shown in Supplemental Figure S10D.

Whole genome bisulfite-seq data processing

Briefly, the whole genome bisulfite-seq data (Supplemental Table S3; Qu et al. 2012) was processed using Trimmomatic (Bolger et al. 2014) and Bismark (Krueger and Andrews 2011), and DNA methylation levels around peak centers were calculated (Supplemental Methods).

Data access

The ChIP-seq, ATAC-seq, and RNA-seq data generated in this study have been submitted to the NCBI BioProject database (https://www.ncbi.nlm.nih.gov/bioproject/) under accession number PRJDB13204 (Supplemental Table S3).

Competing interest statement

The authors declare no competing interests.

Acknowledgments

We acknowledge all the laboratory members for everyday discussion and for their continuous support. This work was supported by Japan Society for the Promotion of Science (JSPS) Grant-in-Aid for JSPS Research Fellow Grant No. JP18J21761 and the Sasakawa Scientific Research Grant from The Japan Science Society to H.S.F., by Japan Agency for Medical Research and Development (AMED) under Grant No. JP18gm1110007h0001 to H.T., and by the JSPS Grant No. JP21K06013 and Grant-in-Aid for Scientific Research on Innovative Areas Grant No. JP21H00245 to R.N.

Author contributions: Conceptualization, investigation, and writing—original draft, H.S.F.; writing—review and editing, H.S.F., H.T., and R.N.; supervision, H.T. and R.N.; funding acquisition, H.S.F., H.T., and R.N.

References

Agger K, Cloos PAC, Christensen J, Pasini D, Rose S, Rappsilber J, Issaeva I, Canaani E, Salcini AE, Helin K. 2007. UTX and JMJD3 are histone H3K27 demethylases involved in *HOX* gene regulation and development. *Nature* **449:** 731–734. doi:10.1038/nature06145

Akkers RC, van Heeringen SJ, Jacobi UG, Janssen-Megens EM, Françoijs K-J, Stunnenberg HG, Veenstra GJC. 2009. A hierarchy of H3K4me3 and H3K27me3 acquisition in spatial gene regulation in xenopus embryos. *Dev Cell* **17:** 425–434. doi:10.1016/j.devcel.2009.08.005

Barski A, Cuddapah S, Cui K, Roh TY, Schones DE, Wang Z, Wei G, Chepelev I, Zhao K. 2007. High-resolution profiling of histone methylations in the human genome. *Cell* **129:** 823–837. doi:10.1016/j.cell.2007.05.009

Bhandari RK. 2016. Medaka as a model for studying environmentally induced epigenetic transgenerational inheritance of phenotypes. *Environ Epigenet* **2:** dvv010. doi:10.1093/eep/dvv010

Blasco MA. 2007. The epigenetic regulation of mammalian telomeres. *Nat Rev Genet* **8:** 299–309. doi:10.1038/nrg2047

Bolger AM, Lohse M, Usadel B. 2014. Trimmomatic: a flexible trimmer for Illumina sequence data. *Bioinformatics* **30:** 2114–2120. doi: 10.1093/bioinformatics/btu170

Bolte S, Cordelières FP. 2006. A guided tour into subcellular colocalization analysis in light microscopy. *J Microsc* **224:** 213–232. doi:10.1111/j.1365-2818.2006.01706.x

Bonhoure N, Bounova G, Bernasconi D, Praz V, Lammers F, Canella D, Willis IM, Herr W, Hernandez N, Delorenzi M, et al. 2014. Quantifying ChIP-seq data: a spiking method providing an internal reference for sample-to-sample normalization. *Genome Res* **24:** 1157–1168. doi:10.1101/gr.168260.113

Chan SH, Tang Y, Miao L, Darwich-Codore H, Vejnar CE, Beaudoin J-D, Musaev D, Fernandez JP, Benitez MDJ, Bazzini AA, et al. 2019. Brd4 and P300 confer transcriptional competency during zygotic genome activation. *Dev Cell* **49:** 867–881.e8. doi:10.1016/j.devcel.2019.05.037

Dahl JA, Jung I, Aanes H, Greggains GD, Manaf A, Lerdrup M, Li G, Kuan S, Li B, Lee AY, et al. 2016. Broad histone H3K4me3 domains in mouse oocytes modulate maternal-to-zygotic transition. *Nature* **537:** 548–552. doi:10.1038/nature19360

Dunleavy E, Pidoux A, Allshire R. 2005. Centromeric chromatin makes its mark. *Trends Biochem Sci* **30:** 172–175. doi:10.1016/j.tibs.2005.02.007

Eckersley-Maslin MA, Alda-Catalinas C, Reik W. 2018. Dynamics of the epigenetic landscape during the maternal-to-zygotic transition. *Nat Rev Mol Cell Biol* **19:** 436–450. doi:10.1038/s41580-018-0008-z

Fukushima HS, Takeda H, Nakamura R. 2019. Targeted in vivo epigenome editing of H3K27me3. *Epigenetics Chromatin* **12:** 17. doi:10.1186/s13072-019-0263-z

Furutani-Seiki M, Wittbrodt J. 2004. Medaka and zebrafish, an evolutionary twin study. *Mech Dev* **121:** 629–637. doi:10.1016/j.mod.2004.05.010

García-Cao M, O'Sullivan R, Peters AHFM, Jenuwein T, Blasco MA. 2004. Epigenetic regulation of telomere length in mammalian cells by the Suv39h1 and Suv39h2 histone methyltransferases. *Nat Genet* **36:** 94–99. doi:10.1038/ng1278

Gonzalo S, Jaco I, Fraga MF, Chen T, Li E, Esteller M, Blasco MA. 2006. DNA methyltransferases control telomere length and telomere recombination in mammalian cells. *Nat Cell Biol* **8:** 416–424. doi:10.1038/ncb1386

Heinz S, Benner C, Spann N, Bertolino E, Lin YC, Laslo P, Cheng JX, Murre C, Singh H, Glass CK. 2010. Simple combinations of lineage-determining transcription factors prime *cis*-regulatory elements required for macrophage and B cell identities. *Mol Cell* **38:** 576–589. doi:10.1016/j.molcel.2010.05.004

Hickey GJ, Wike CL, Nie X, Guo Y, Tan M, Murphy PJ, Cairns BR. 2022. Establishment of developmental gene silencing by ordered polycomb complex recruitment in early zebrafish embryos. *eLife* **11:** e67738. doi:10.7554/eLife.67738

Hogg SJ, Motorna O, Cluse LA, Johanson TM, Coughlan HD, Raviram R, Myers RM, Costacurta M, Todorovski I, Pijpers L, et al. 2021. Targeting histone acetylation dynamics and oncogenic transcription by catalytic P300/CBP inhibition. *Mol Cell* **81:** 2183–2200.e13. doi:10.1016/j.molcel.2021.04.015

Hontelez S, van Kruijsbergen I, Georgiou G, van Heeringen SJ, Bogdanovic O, Lister R, Veenstra GJC. 2015. Embryonic transcription is controlled by maternally defined chromatin state. *Nat Commun* **6:** 10148. doi:10.1038/ncomms10148

Hunt G, Boija A, Mannervik M. 2022. p300/CBP sustains Polycomb silencing by non-enzymatic functions. *Mol Cell* **82:** 3580–3597.e9. doi:10.1016/j.molcel.2022.09.005

Ichikawa K, Tomioka S, Suzuki Y, Nakamura R, Doi K, Yoshimura J, Kumagai M, Inoue Y, Uchida Y, Irie N, et al. 2017. Centromere evolution and CpG methylation during vertebrate speciation. *Nat Commun* **8:** 1833. doi:10.1038/s41467-017-01982-7

Inoue A, Jiang L, Lu F, Suzuki T, Zhang Y. 2017. Maternal H3K27me3 controls DNA methylation-independent imprinting. *Nature* **547:** 419–424. doi:10.1038/nature23262

Iwamatsu T. 2004. Stages of normal development in the medaka *Oryzias latipes*. *Mech Dev* **121:** 605–618. doi:10.1016/j.mod.2004.03.012

Jang MK, Mochizuki K, Zhou M, Jeong H-S, Brady JN, Ozato K. 2005. The bromodomain protein Brd4 is a positive regulatory component of P-TEFb and stimulates RNA polymerase II-dependent transcription. *Mol Cell* **19:** 523–534. doi:10.1016/j.molcel.2005.06.027

Jiang L, Zhang J, Wang JJ, Wang L, Zhang L, Li G, Yang X, Ma X, Sun X, Cai J, et al. 2013. Sperm, but not oocyte, DNA methylome is inherited by zebrafish early embryos. *Cell* **153:** 773–784. doi:10.1016/j.cell.2013.04.041

Jukam D, Shariati SAM, Skotheim JM. 2017. Zygotic genome activation in vertebrates. *Dev Cell* **42:** 316–332. doi:10.1016/j.devcel.2017.07.026

Jullien J, Vodnala M, Pasque V, Oikawa M, Miyamoto K, Allen G, David SA, Brochard V, Wang S, Bradshaw C, et al. 2017. Gene resistance to transcriptional reprogramming following nuclear transfer is directly mediated by multiple chromatin-repressive pathways. *Mol Cell* **65:** 873–884.e8. doi:10.1016/j.molcel.2017.01.030

Kinoshita M, Murata K, Naruse K, Tanaka M. 2009. *Medaka: biology, management, and experimental protocols*. Wiley-Blackwell, Ames, IA.

Krueger F, Andrews SR. 2011. Bismark: a flexible aligner and methylation caller for Bisulfite-Seq applications. *Bioinformatics* **27:** 1571–1572. doi:10.1093/bioinformatics/btr167

Ku M, Koche RP, Rheinbay E, Mendenhall EM, Endoh M, Mikkelsen TS, Presser A, Nusbaum C, Xie X, Chi AS, et al. 2008. Genomewide analysis of PRC1 and PRC2 occupancy identifies two classes of bivalent domains. *PLoS Genet* **4:** e1000242. doi:10.1371/journal.pgen.1000242

Lasko LM, Jakob CG, Edalji RP, Qiu W, Montgomery D, Digiammarino EL, Hansen TM, Risi RM, Frey R, Manaves V, et al. 2017. Discovery of a selective catalytic p300/CBP inhibitor that targets lineage-specific tumours. *Nature* **550:** 128–132. doi:10.1038/nature24028

Laue K, Rajshekar S, Courtney AJ, Lewis ZA, Goll MG. 2019. The maternal to zygotic transition regulates genome-wide heterochromatin establishment in the zebrafish embryo. *Nat Commun* **10:** 1551. doi:10.1038/s41467-019-09582-3

Li X-Y, Harrison MM, Villalta JE, Kaplan T, Eisen MB. 2014. Establishment of regions of genomic activity during the *Drosophila* maternal to zygotic transition. *eLife* **3:** e03737. doi:10.7554/eLife.03737

Li Y, Liu Y, Yang H, Zhang T, Naruse K, Tu Q. 2020. Dynamic transcriptional and chromatin accessibility landscape of medaka embryogenesis. *Genome Res* **30:** 924–937. doi:10.1101/gr.258871.119

Lindeman LC, Andersen IS, Reiner AH, Li N, Aanes H, Østrup O, Winata C, Mathavan S, Müller F, Alestrom P, et al. 2011. Prepatterning of developmental gene expression by modified histones before zygotic genome activation. *Dev Cell* **21:** 993–1004. doi:10.1016/j.devcel.2011.10.008

Love MI, Huber W, Anders S. 2014. Moderated estimation of fold change and dispersion for RNA-seq data with DESeq2. *Genome Biol* **15:** 550. doi:10.1186/s13059-014-0550-8

Lu X, Zhang Y, Wang L, Wang L, Wang H, Xu Q, Xiang Y, Chen C, Kong F, Xia W, et al. 2021. Evolutionary epigenomic analyses in mammalian early embryos reveal species-specific innovations and conserved principles of imprinting. *Sci Adv* **7:** eabi6178. doi:10.1126/sciadv.abi6178

Luo X, Ou Y, Li R, He Y. 2020. Maternal transmission of the epigenetic 'memory of winter cold' in *Arabidopsis*. *Nat Plants* **6:** 1211–1218. doi:10.1038/s41477-020-00774-0

Maciejowski J, Li Y, Bosco N, Campbell PJ, de Lange T. 2015. Chromothripsis and kataegis induced by telomere crisis. *Cell* **163:** 1641–1654. doi:10.1016/j.cell.2015.11.054

Macleod D, Clark VH, Bird A. 1999. Absence of genome-wide changes in DNA methylation during development of the zebrafish. *Nat Genet* **23:** 139–140. doi:10.1038/13767

Macrae TA, Fothergill-Robinson J, Ramalho-Santos M. 2022. Regulation, functions and transmission of bivalent chromatin during mammalian development. *Nat Rev Mol Cell Biol* **24:** 6–26. doi:10.1038/s41580-022-00518-2

Martire S, Gogate AA, Whitmill A, Tafessu A, Nguyen J, Teng Y-C, Tastemel M, Banaszynski LA. 2019. Phosphorylation of histone H3.3 at serine 31 promotes p300 activity and enhancer acetylation. *Nat Genet* **51:** 941–946. doi:10.1038/s41588-019-0428-5

Matoba S, Liu Y, Lu F, Iwabuchi KA, Shen L, Inoue A, Zhang Y. 2014. Embryonic development following somatic cell nuclear transfer impeded by persisting histone methylation. *Cell* **159:** 884–895. doi:10.1016/j.cell.2014.09.055

Mendenhall EM, Koche RP, Truong T, Zhou VW, Issac B, Chi AS, Ku M, Bernstein BE. 2010. GC-rich sequence elements recruit PRC2 in mammalian ES cells. *PLoS Genet* **6:** e1001244. doi:10.1371/journal.pgen.1001244

Mi H, Muruganujan A, Ebert D, Huang X, Thomas PD. 2019. PANTHER version 14: more genomes, a new PANTHER GO-slim and improvements in enrichment analysis tools. *Nucleic Acids Res* **47:** D419–D426. doi:10.1093/nar/gky1038

Miao L, Tang Y, Bonneau AR, Chan SH, Kojima ML, Pownall ME, Vejnar CE, Gao F, Krishnaswamy S, Hendry CE, et al. 2022. The landscape of pioneer factor activity reveals the mechanisms of chromatin reprogramming and genome activation. *Mol Cell* **82:** 986–1002.e9. doi:10.1016/j.molcel.2022.01.024

Murphy PJ, Wu SF, James CR, Wike CL, Cairns BR. 2018. Placeholder nucleosomes underlie germline-to-embryo DNA methylation reprogramming. *Cell* **172:** 993–1006.e13. doi:10.1016/j.cell.2018.01.022

Murphy KE, Meng FW, Makowski CE, Murphy PJ. 2020. Genome-wide chromatin accessibility is restricted by ANP32E. *Nat Commun* **11:** 5063. doi:10.1038/s41467-020-18821-x

Nakamura R, Tsukahara T, Qu W, Ichikawa K, Otsuka T, Ogoshi K, Saito TL, Matsushima K, Sugano S, Hashimoto S, et al. 2014. Large

hypomethylated domains serve as strong repressive machinery for key developmental genes in vertebrates. *Development* **141:** 2568–2580. doi:10.1242/dev.108548

Nakamura R, Motai Y, Kumagai M, Wike CL, Nishiyama H, Nakatani Y, Durand NC, Kondo K, Kondo T, Tsukahara T, et al. 2021. CTCF looping is established during gastrulation in medaka embryos. *Genome Res* **31:** 968–980. doi:10.1101/gr.269951.120

Narita T, Ito S, Higashijima Y, Chu WK, Neumann K, Walter J, Satpathy S, Liebner T, Hamilton WB, Maskey E, et al. 2021. Enhancers are activated by p300/CBP activity-dependent PIC assembly, RNAPII recruitment, and pause release. *Mol Cell* **81:** 2166–2182.e6. doi:10.1016/j.molcel.2021.03.008

Ohta S, Wood L, Bukowski-Wills J-C, Rappsilber J, Earnshaw WC. 2011. Building mitotic chromosomes. *Curr Opin Cell Biol* **23:** 114–121. doi:10.1016/j.ceb.2010.09.009

Orlando DA, Chen MW, Brown VE, Solanki S, Choi YJ, Olson ER, Fritz CC, Bradner JE, Guenther MG. 2014. Quantitative ChIP-Seq normalization reveals global modulation of the epigenome. *Cell Rep* **9:** 1163–1170. doi:10.1016/j.celrep.2014.10.018

O'Sullivan RJ, Karlseder J. 2010. Telomeres: protecting chromosomes against genome instability. *Nat Rev Mol Cell Biol* **11:** 171–181. doi:10.1038/nrm2848

Pelham-Webb B, Polyzos A, Wojenski L, Kloetgen A, Li J, Di Giammartino DC, Sakellaropoulos T, Tsirigos A, Core L, Apostolou E. 2021. H3k27ac bookmarking promotes rapid post-mitotic activation of the pluripotent stem cell program without impacting 3D chromatin reorganization. *Mol Cell* **81:** 1732–1748.e8. doi:10.1016/j.molcel.2021.02.032

Perino M, van Mierlo G, Karemaker ID, van Genesen S, Vermeulen M, Marks H, van Heeringen SJ, Veenstra GJC. 2018. MTF2 recruits Polycomb Repressive Complex 2 by helical-shape-selective DNA binding. *Nat Genet* **50:** 1002–1010. doi:10.1038/s41588-018-0134-8

Perino M, van Mierlo G, Loh C, Wardle SMT, Zijlmans DW, Marks H, Veenstra GJC. 2020. Two functional axes of feedback-enforced PRC2 recruitment in mouse embryonic stem cells. *Stem Cell Reports* **15:** 1287–1300. doi:10.1016/j.stemcr.2020.07.007

Piunti A, Shilatifard A. 2016. Epigenetic balance of gene expression by Polycomb and COMPASS families. *Science* **352:** aad9780. doi:10.1126/science.aad9780

Potok ME, Nix DA, Parnell TJ, Cairns BR. 2013. Reprogramming the maternal zebrafish genome after fertilization to match the paternal methylation pattern. *Cell* **153:** 759–772. doi:10.1016/j.cell.2013.04.030

Qu W, Hashimoto S, Shimada A, Nakatani Y, Ichikawa K, Saito TL, Ogoshi K, Matsushima K, Suzuki Y, Sugano S, et al. 2012. Genome-wide genetic variations are highly correlated with proximal DNA methylation patterns. *Genome Res* **22:** 1419–1425. doi:10.1101/gr.140236.112

Quevedo M, Meert L, Dekker MR, Dekkers DHW, Brandsma JH, van den Berg DLC, Ozgür Z, van IJcken WFJ, Demmers J, Fornerod M, et al. 2019. Mediator complex interaction partners organize the transcriptional network that defines neural stem cells. *Nat Commun* **10:** 2669. doi:10.1038/s41467-019-10502-8

Rosenfeld JA, Wang Z, Schones DE, Zhao K, DeSalle R, Zhang MQ. 2009. Determination of enriched histone modifications in non-genic portions of the human genome. *BMC Genomics* **10:** 143. doi:10.1186/1471-2164-10-143

Rougeot J, Chrispijn ND, Aben M, Elurbe DM, Andralojc KM, Murphy PJ, Jansen PWTC, Vermeulen M, Cairns BR, Kamminga LM. 2019. Maintenance of spatial gene expression by Polycomb-mediated repression after formation of a vertebrate body plan. *Development* **146:** dev178590. doi:10.1242/dev.178590

Sato Y, Hilbert L, Oda H, Wan Y, Heddleston JM, Chew T-L, Zaburdaev V, Keller P, Lionnet T, Vastenhouw N, et al. 2019. Histone H3K27 acetylation precedes active transcription during zebrafish zygotic genome activation as revealed by live-cell analysis. *Development* **146:** dev179127. doi:10.1242/dev.179127

Schindelin J, Arganda-Carreras I, Frise E, Kaynig V, Longair M, Pietzsch T, Preibisch S, Rueden C, Saalfeld S, Schmid B, et al. 2012. Fiji: an open-source platform for biological-image analysis. *Nat Methods* **9:** 676–682. doi:10.1038/nmeth.2019

Schuettengruber B, Bourbon H-M, Di Croce L, Cavalli G. 2017. Genome regulation by Polycomb and Trithorax: 70 years and counting. *Cell* **171:** 34–57. doi:10.1016/j.cell.2017.08.002

Shao F, Han M, Peng Z. 2019. Evolution and diversity of transposable elements in fish genomes. *Sci Rep* **9:** 15399. doi:10.1038/s41598-019-51888-1

Shvedunova M, Akhtar A. 2022. Modulation of cellular processes by histone and non-histone protein acetylation. *Nat Rev Mol Cell Biol* **23:** 329–349. doi:10.1038/s41580-021-00441-y

Stewart-Morgan KR, Petryk N, Groth A. 2020. Chromatin replication and epigenetic cell memory. *Nat Cell Biol* **22:** 361–371. doi:10.1038/s41556-020-0487-y

Takeda H, Shimada A. 2010. The art of medaka genetics and genomics: What makes them so unique? *Annu Rev Genet* **44:** 217–241. doi:10.1146/annurev-genet-051710-151001

Tie F, Banerjee R, Stratton CA, Prasad-Sinha J, Stepanik V, Zlobin A, Diaz MO, Scacheri PC, Harte PJ. 2009. CBP-mediated acetylation of histone H3 lysine 27 antagonizes *Drosophila* Polycomb silencing. *Development* **136:** 3131–3141. doi:10.1242/dev.037127

Umbreit NT, Zhang C-Z, Lynch LD, Blaine LJ, Cheng AM, Tourdot R, Sun L, Almubarak HF, Judge K, Mitchell TJ, et al. 2020. Mechanisms generating cancer genome complexity from a single cell division error. *Science* **368:** eaba0712. doi:10.1126/science.aba0712

van Mierlo G, Veenstra GJC, Vermeulen M, Marks H. 2019. The complexity of PRC2 subcomplexes. *Trends Cell Biol* **29:** 660–671. doi:10.1016/j.tcb.2019.05.004

Vastenhouw NL, Zhang Y, Woods IG, Imam F, Regev A, Liu XS, Rinn J, Schier AF. 2010. Chromatin signature of embryonic pluripotency is established during genome activation. *Nature* **464:** 922–926. doi:10.1038/nature08866

Veenstra GJC, Wolffe AP. 2001. Constitutive genomic methylation during embryonic development of *Xenopus*. *Biochim Biophys Acta* **1521:** 39–44. doi:10.1016/S0167-4781(01)00280-9

Wang C, Liu X, Gao Y, Yang L, Li C, Liu W, Chen C, Kou X, Zhao Y, Chen J, et al. 2018. Reprogramming of H3K9me3-dependent heterochromatin during mammalian embryo development. *Nat Cell Biol* **20:** 620–631. doi:10.1038/s41556-018-0093-4

Xia W, Xie W. 2020. Rebooting the epigenomes during mammalian early embryogenesis. *Stem Cell Reports* **15:** 1158–1175. doi:10.1016/j.stemcr.2020.09.005

Xia W, Xu J, Yu G, Yao G, Xu K, Ma X, Zhang N, Liu B, Li T, Lin Z, et al. 2019. Resetting histone modifications during human parental-to-zygotic transition. *Science* **365:** 353–360. doi:10.1126/science.aaw5118

Xiang Y, Zhu Z, Han G, Lin H, Xu L, Chen CD. 2007. JMJD3 is a histone H3K27 demethylase. *Cell Res* **17:** 850–857. doi:10.1038/cr.2007.83

Zenk F, Loeser E, Schiavo R, Kilpert F, Bogdanović O, Iovino N. 2017. Germ line–inherited H3K27me3 restricts enhancer function during maternal-to-zygotic transition. *Science* **357:** 212–216. doi:10.1126/science.aam5339

Zhang Y, Liu T, Meyer CA, Eeckhoute J, Johnson DS, Bernstein BE, Nusbaum C, Myers RM, Brown M, Li W, et al. 2008. Model-based Analysis of ChIP-Seq (MACS). *Genome Biol* **9:** R137. doi:10.1186/gb-2008-9-9-r137

Zhang B, Zheng H, Huang B, Li W, Xiang Y, Peng X, Ming J, Wu X, Zhang Y, Xu Q, et al. 2016. Allelic reprogramming of the histone modification H3K4me3 in early mammalian development. *Nature* **537:** 553–557. doi:10.1038/nature19361

Zhang B, Wu X, Zhang W, Shen W, Sun Q, Liu K, Zhang Y, Wang Q, Li Y, Meng A, et al. 2018a. Widespread enhancer dememorization and promoter priming during parental-to-zygotic transition. *Mol Cell* **72:** 673–686.e6. doi:10.1016/j.molcel.2018.10.017

Zhang Y, Wang Q, Liu K, Gao E, Guan H, Hou J. 2018b. Treatment of donor cells with recombinant KDM4D protein improves preimplantation development of cloned ovine embryos. *Cytotechnology* **70:** 1469–1477. doi:10.1007/s10616-018-0224-6

Zhao W, Xu Y, Wang Y, Gao D, King J, Xu Y, Liang F-S. 2021. Investigating crosstalk between H3K27 acetylation and H3K4 trimethylation in CRISPR/dCas-based epigenome editing and gene activation. *Sci Rep* **11:** 15912. doi:10.1038/s41598-021-95398-5

Zhou VW, Goren A, Bernstein BE. 2011. Charting histone modifications and the functional organization of mammalian genomes. *Nat Rev Genet* **12:** 7–18. doi:10.1038/nrg2905

Received December 7, 2022; accepted in revised form March 29, 2023.